THE JOURNAL OF PHYSICAL CHEMISTRY C
A JOURNAL OF THE AMERICAN CHEMICAL SOCIETY

pubs.acs.org/JPCC

Article

Plasmon-Induced Vibrational Circular Dichroism Bands of Achiral Molecules on Gold Nanostructures with Tunable Extrinsic Chiroptical Responses

Amy Morren, Aria T. Ballance, Flore K. Elliott, and Jennifer S. Shumaker-Parry*

Cite This: J. Phys. Chem. C 2024, 128, 15091−15102

Read Online

ACCESS | Metrics & More | Article Recommendations | Supporting Information

Downloaded via UNIV OF UTAH on November 27, 2024 at 20:26:04 (UTC).
See https://pubs.acs.org/sharingguidelines for options on how to legitimately share published articles.

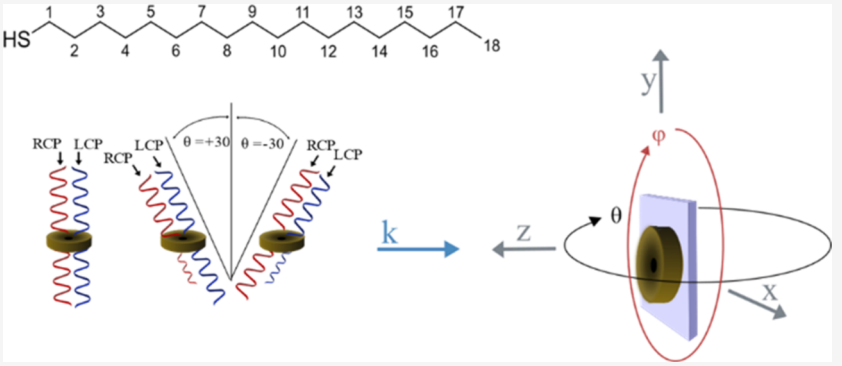

ABSTRACT: Vibrational circular dichroism (VCD) is an important method used to assign absolute configuration to chiral molecules, but inherently weak signals necessitate high concentrations and long acquisition times for analysis. Plasmonic nanostructures are of interest for enhancement of VCD signals. However, understanding the influence of plasmonic structures on molecular VCD spectral features is important for assessing the information content of the spectra. Here, we present a study of plasmonic gold nanobowl hole (NBH) structures and the influence on the VCD spectra of achiral molecules. VCD bands for the symmetric and antisymmetric methylene stretching modes of 1-octadecanethiol (ODT) on NBHs were observed. Measurements of ODT on CaF_2 substrates without plasmonic structures confirmed that the bands were not an artifact of tilting the substrate. The handedness of the VCD bands showed an inverse dependence on the handedness of the extrinsic CD response of the NBHs, producing a relative handedness of the opposite sign. By controlling the size of the NBHs, the localized surface plasmon resonance (LSPR) and CD bands were tuned relative to the spectral position of the ODT VCD bands. The amplitude and line shape of the methylene stretch VCD bands showed a strong dependence on overlap with the plasmonic CD band in the same spectral region. To further investigate the origin of the molecular VCD bands, nanobowls without holes (NBs) and nanodisks (NDs) were fabricated. The LSPR behavior of NBs and NDs was similar to NBHs, but the structures did not exhibit the extrinsic CD responses of NBHs, evidenced by the lack of defined CD bands and handedness conversion. Although the NBs and NDs exhibited small CD signals, VCD bands were not observed for ODT on the NBs and NDs. Stearic acid (SA) on NBHs also produced VCD bands, demonstrating the influence of the plasmonic nanostructures on molecules with different surface interactions and organization. Asymmetric line shapes of the VCD bands of ODT appeared similar to Fano resonance line shapes observed in surface-enhanced infrared absorption (SEIRA) spectroscopy; however, the NBH CD response was shown to be a key factor in producing the VCD bands, rather than the primary LSPR that influences the line shapes and enhancements in SEIRA. The studies of VCD spectra of achiral molecules on plasmonic structures highlight the importance of understanding how the plasmonic and chiroptical behaviors of the substrates impact the spectral features used to identify enantiomers in VCD spectroscopy, especially for configuration analysis and comparison with quantum calculations.

INTRODUCTION

Chirality is an important characteristic of molecules and macroscopic structures in which an entity possesses a nonsuperimposable mirror image, with two such mirror images known as enantiomers. The identity of an enantiomer of a chiral compound has far-reaching implications for biological processes, which are often enantiospecific.[1−3] Thus, differ-

Received: July 3, 2024
Revised: August 21, 2024
Accepted: August 22, 2024
Published: September 2, 2024

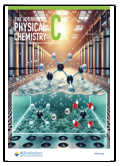

ACS Publications
© 2024 American Chemical Society

entiation between enantiomers is necessary to assess the enantiomeric purity in enantioselective reactions and separations, particularly in the development of therapeutics for medical conditions.[4−6] Chiroptical properties of chiral molecules, such as differential absorption of circularly polarized light (i.e., circular dichroism, CD), are used to distinguish between two enantiomers of a chiral compound. Vibrational circular dichroism spectroscopy (VCD) is the extension of CD spectroscopy, more commonly measured in the ultraviolet and visible spectral regions, into the infrared (IR). VCD is used to assign absolute configuration and conformational population distribution of enantiomers.[7−12] One challenge with applying this spectroscopy method is that VCD signals are 4 to 5 orders of magnitude lower than the parent IR absorption signals.[13] As a result, high concentrations of molecules and long acquisition times are required for VCD analysis.

Chiroptical behavior in plasmonic systems is a relatively new area of research that is promising for enhancement of chiroptical spectroscopies of molecular systems.[14−23] The tunability of nano- to microscale features in plasmonic nanostructures provides access to a broad range of chiroptical behavior.[21,24−26] Plasmonic enhancement of VCD signals of molecules has been the focus of several research reports.[27−30] For example, Knipper et al. fabricated thin gold and titanium films with arrays of asymmetric angled crossed slits that showed large CD response in the IR spectral region.[27] When R- or S-α-pinene was deposited on the substrates, there was a large change in the shape and a spectral shift of the plasmonic band observed in the VCD spectrum of the slit arrays that was discernably different for the two enantiomers. In another example, Xu et al. fabricated a perpendicularly positioned two-resonator system with both in-plane and out-of-plane asymmetry contributing to predicted chiral optical near fields due to coupling between the resonators.[28] They found that the bovine serum albumin (BSA) and β-lactoglobulin amide vibrational bands in the ∼1600 cm^{-1} region produced opposite VCD signals that coupled differentially with left- or right-handed structures. Xu et al. also fabricated an arrangement of coupled quadruple-resonator structures predicted to have a weaker plasmonic chiroptical response with respect to the enhanced and reflected VCD molecular response of adsorbed L- and D-glucose.[29] In that study, they reported that the local chiroptical behavior of the coupled resonators within a structure unit could affect the chiral response of molecules located within that environment based on the VCD spectra. In addition to signal enhancements, the impact on the shape of molecular VCD bands was emphasized by work from Biswas et al. The group fabricated reflective gold disk-hole square arrays with predicted chiral optical near fields with zero far-field CD response due to the achiral nature of the structured array.[30] They found that VCD responses from L- and D-thalidomide were enhanced on the achiral hole-disks. However, the VCD bands and intensities changed when the radii of the hole-disks were controlled to tune the localized surface plasmon resonance (LSPR) response of the hole-disk arrays, thus impacting the chiral plasmonic electromagnetic near fields. These studies demonstrated the potential of plasmonic platforms to enhance the VCD signals of molecules, but the research also highlighted the challenges associated with plasmon-enhanced VCD, specifically the dependence of the VCD band shapes and enhancements on the coupling with the chiral plasmonic near field. The plasmonic effects must be well understood to extract the detailed structural and conformational information needed for absolute configuration assignment and determination of population distribution in plasmon-enhanced VCD platforms.[27]

To gain insight into how plasmonic structures impact VCD signals, we used a tunable plasmonic platform with extrinsic chiroptical response to study the influence of IR CD response of plasmonic substrates on the VCD spectra of an achiral molecule, 1-octadecanethiol (ODT). Nanobowl hole (NBH) arrays provided a two-fold tunability in the optical response. First, the LSPR response of the NBH arrays was tuned to the IR spectral range by controlling the diameter of the structures. Second, the IR CD response of the NBHs was manipulated using angle-based measurements. Due to the offset hole in the bowl-shaped structure and the resulting geometric anisotropy, NBHs exhibit extrinsic chirality. At normal incidence, the structures exhibit no CD response. However, at tilted angles with respect to the incident light, the structures undergo full handedness conversion, from left-handed to right-handed, demonstrating a CD response due to extrinsic chirality.[21,31−36] This tunable NBH plasmonic platform was used to study the VCD spectra of ODT adsorbed on the NBHs with a focus on the spectral region of the methylene symmetric and antisymmetric stretch vibrational bands. The influence of the optical behavior of NBHs on the VCD spectra of ODT was compared to nanobowls (NBs) and nanodisks (NDs) to explore the origin of the VCD bands and the influence of the LSPR and chiroptical response of the plasmonic structures. To probe the potential role of molecular organization and surface interactions, the VCD spectra of stearic acid (SA) on the NBHs was compared to the VCD of ODT.

METHODS

Materials. Stearic acid (SA, ≥98.5%) and 1-octadecanethiol (ODT) were purchased from Sigma-Aldrich. Ethanol (200 proof) was purchased from Deacon Laboratories, Inc. Acetone and isopropyl alcohol (both reagent grade) were purchased from Fisher Scientific. Polystyrene (PS) beads were purchased from Polysciences, Inc. Calcium fluoride (CaF_2) substrates (25.5 mm diameter; 2 mm thickness) were purchased from OptoCity (Raleigh, NC). Nanopure water was purified to 18 MΩ using a Barnstead NanopureDiamond system.

Fabrication of Plasmonic Structures. Nanosphere template lithography (NTL) was used to fabricate plasmonic structures in an ISO 7 cleanroom.[21,37,38] For fabrication of the NBH arrays, CaF_2 substrates were cleaned by copious rinsing with acetone, isopropyl alcohol, and ethanol before drying with nitrogen followed by 5 min of UVO cleaning (Jelight Company, Inc.) on each substrate face for a total of 10 min. The clean CaF_2 substrates were submerged in Nanopure water. An aliquot of a stock of PS beads of a selected size was mixed with ethanol at a 1:1 volume ratio. To deposit the PS beads, the ethanol-diluted solution of PS beads was collected at the air−water interface above the submerged CaF_2 substrates using a ramp and an automatic syringe (New Era Pump Systems, Inc.) dispensing the solution at a rate of 0.25 μL/min. After a monolayer of PS beads was formed at the air−water interface above the CaF_2 substrates, the water was removed using a peristaltic pump (ISMATEC) and the substrates with PS beads deposited were left to dry overnight. The deposition produced a close-packed monolayer of PS beads on the CaF_2 substrates. The PS beads on CaF_2 were etched with oxygen plasma (Oxford 80 Plasmalab) to reduce the individual bead size to

https://doi.org/10.1021/acs.jpcc.4c04448
J. Phys. Chem. C 2024, 128, 15091−15102

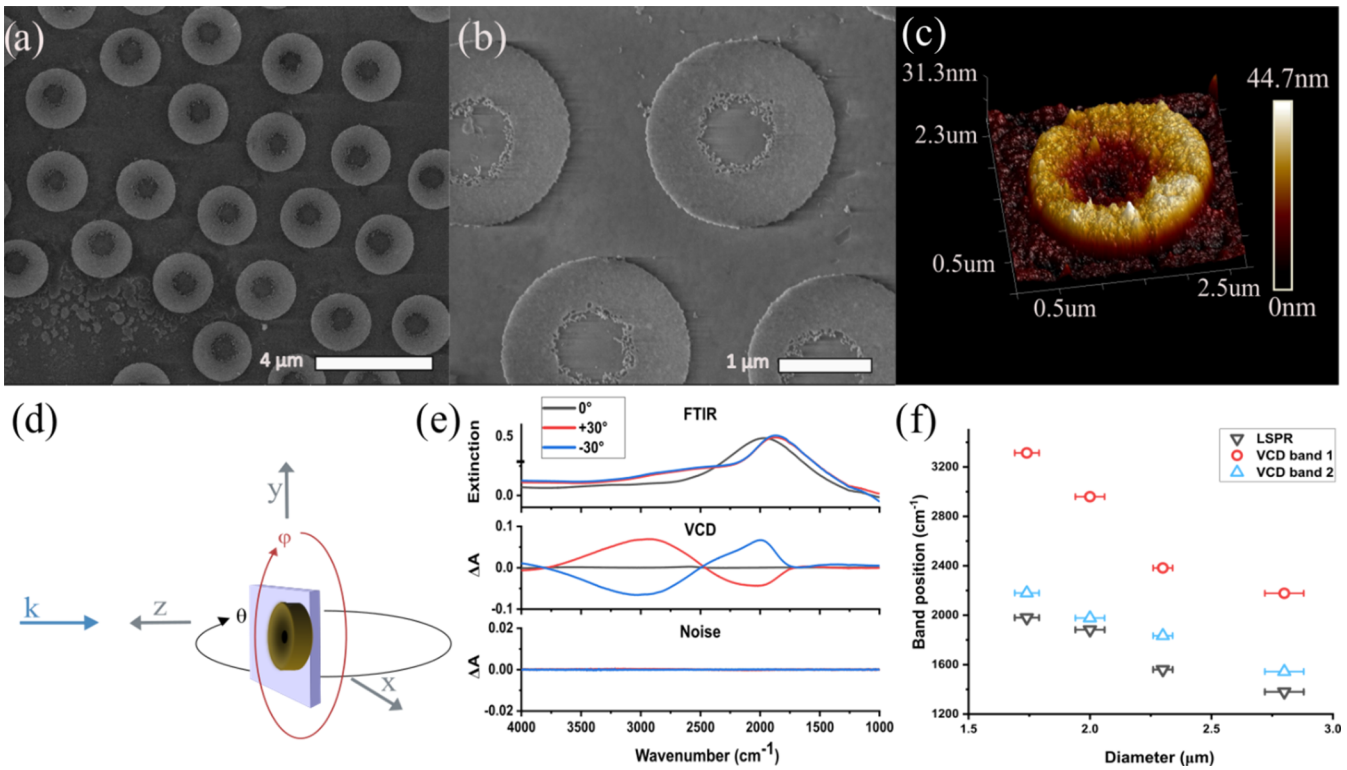

Figure 1. Structural and optical characterization of NBH structures. (a) Low magnification and (b) high magnification SEM images of 2.00-μm-diameter Au NBHs. (c) AFM height image of a 2.00 μm NBH. (d) Illustration of the axes of orientation for gold NBHs on a substrate with respect to incident wavevector, k, with in-plane rotation, ϕ, and out-of-plane rotation, θ. Here, the wavevector, k, is traveling in the $-z$ direction, in-plane rotations in ϕ are in the xy plane at normal incidence and out-of-plane rotations in θ are in the xz plane. (e) FTIR, VCD, and VCD noise spectra for a 2.00 μm NBH array at normal incidence ($\theta = 0°$) in black, $\theta = +30°$ in red, and $\theta = -30°$ blue. (f) Relationship of the LSPR and VCD bands with the outer diameter of Au NBHs. The center spectral position for the dominant LSPR band (black triangles), the center of the higher energy VCD band 1 (red circles), and center of the lower energy VCD band 2 (blue triangles) were found to depend on the NBH outer diameter. Error bars represent 1 standard deviation for the diameter measurements based on 20 measurements of at least 10 structures.

the target diameter of the NBH structures. A 4″ gold target from Denton Vacuum with 99.99% purity was used in a Denton 635 to sputter deposit a 30−40 nm-thick gold film on the etched PS beads, followed by argon ion (Ar^+) milling at normal incidence using the Oxford 80 Plasmalab. Removal of the PS beads using tape left an array of randomly organized regions of close-packed NBH structures. Each NBH had a concave bowl shape with a hole where the PS bead template blocked gold deposition on the substrate during fabrication.

To fabricate NB and ND arrays, a thin gold film of 10 nm for NB arrays and 30 nm for ND arrays was deposited on the CaF_2 substrate before the deposition of the PS beads. The film formed the bottom of the bowls without holes (i.e., NBs) and the height of the disks (i.e., NDs). For the NB array, PS beads were deposited onto the 10 nm-thick gold film and were etched with oxygen plasma to the desired diameter. To reach a structure height of 30 nm, another 20 nm-thick gold film was deposited on top of the initial 10 nm-thick gold film and PS beads before Ar^+ milling at normal incidence was performed using the Oxford 80 Plasmalab. Removal of the PS beads resulted in an array of gold NBs. For the ND structures, a 30 nm-thick gold film was deposited before PS bead deposition. After oxygen plasma etching of the PS beads, the continuous gold film surrounding the PS beads was removed with Ar^+ milling at normal incidence, with the gold directly under the bead protected during the etching process. Removal of the PS beads using tape resulted in an array of NDs.

Deposition of ODT and SA. Plasmonic substrates were cleaned prior to molecule deposition by rinsing with acetone, isopropanol, and ethanol in order of decreasing polarity before cleaning with a UV-Ozone cleaner for 5 min on each side for a total of 10 min. A 1%w/v solution of ODT in ethanol was prepared. The NBH arrays were incubated in the ODT solution for 18 h, rinsed with 1−3 mL of ethanol, dried with nitrogen, and measured immediately. For deposition of ODT on CaF_2, a 50 μL aliquot of the 1%w/v solution of ODT in ethanol was drop cast on the substrate, and the solvent was allowed to evaporate. For SA deposition, a 1 mM solution of SA in ethanol was prepared and 50 μL was drop cast onto a clean NBH array and allowed to dry completely before measurement.

Structural Characterization. Scanning electron microscopy (SEM) was performed using an FEI Nova Nano630 SEM in immersion mode using a Helix detector. NBH inner hole diameters, outer structure diameters, and structure density on the substrate were analyzed using 20 measurements per type of structure using ImageJ. See Figure S1 in the Supporting Information for example SEM images. Atomic force microscopy (AFM) was conducted using a Bruker Dimension Icon AFM with Veeco ScanAsyst in ScanAsyst mode that enabled auto-optimization of scanning parameters in peak force tapping mode. A Veeco ScanAsyst-air probe with a silicon tip on a silicon nitride lever was used for imaging, and NanoScope Analysis 2.0 software was used to process the AFM data.

https://doi.org/10.1021/acs.jpcc.4c04448
J. Phys. Chem. C 2024, 128, 15091−15102

Spectroscopy Measurements. For optical characterization of the plasmonic nanostructures, Fourier-transform infrared (FTIR) and VCD spectra were measured using a ChiralIR-2X VCD spectrometer from BioTools, Inc. The VCD spectra were produced using the FT-VCD instrument with dual photoelastic modulators (PEMs).[12,39] The FTIR spectra and VCD spectra were measured simultaneously. For VCD, the spectrum is presented as a difference spectrum for the sample interaction with left- vs right-circularly polarized light. Therefore, a positive difference in absorption indicates a left-handed response and a negative difference indicates a right-handed response. The FTIR and VCD spectra were collected using angle control of the substrate with a fine-tuning indexing rotational mount (Thorlabs) and a fine-tuning indexing rotational base (Edmund Optics). The illustration in Figure 1d shows the substrate in-plane rotation angle (ϕ) and out-of-plane tilt angle (θ) defined with respect to the incident light k vector which was orthogonal to the plane of incidence at θ = 0°. Parent FTIR spectra were acquired in blocks of 50 scans at each 15° increment of in-plane rotation (ϕ = 15°) for a total of 24 in-plane measurements at each incident angle (θ = 0, ±30°). To reduce linear dichroism contributions to the VCD spectra, the spectra collected for the in-plane measurements were averaged. The VCD software automatically produced the FTIR, VCD and noise spectra. The VCD spectra were the result of adding the spectra produced during the forward and backward scans of the interferometer and dividing by two. The noise spectrum was produced by subtracting the spectra from the forward and backward scans and dividing by two. The noise spectrum represents the baseline of the VCD, and a featureless spectrum indicates a lack of artifacts from the optical system of the spectrometer. The same procedure was used to collect FTIR and VCD spectra for a bare CaF_2 substrate, and these spectra were used for background correction by subtracting the averaged CaF_2 FTIR and VCD spectra from the corresponding averaged sample measurements. The methods for FTIR and VCD analysis of ODT and SA on the NBH arrays were identical to measurement of the FTIR and VCD spectra for NBH structures. Note: The IR CD spectra obtained for the plasmonic nanostructures without ODT or SA are referred to as VCD spectra to be consistent with previous literature and to simplify the discussion.

RESULTS AND DISCUSSION

Investigations of the coupling of achiral molecules with plasmonic structures with chiroptical responses utilized NBH structures as a tunable plasmonic platform. SEM images of NBHs in Figure 1a,b show the 2-μm-diameter structures have a circular base with a hole where the CaF_2 substrate is exposed. The AFM image of a NBH in Figure 1c shows the three-dimensional shape of the structure, which is not flat, but instead has a curved concave bowl surface that recedes to the hole in the center. The PS bead template determined the structural features of the NBHs. The hole was the result of the PS bead blocking that area of the substrate during metal deposition, while the gold bowl was formed by the spherical bead protecting the gold material during Ar^+ milling. The AFM height image shows that the hole is offset within the structure due to the angle-based metal deposition, which is the result of the position of the substrate holder relative to the metal source.

To assess the LSPR and chiroptical responses of the plasmonic structures, measurements were made with the NBH array substrate normal (θ = 0°) to the incident light and with the substrate tilted at θ = ±30° (see Figure 1e). The angle-dependent measurement details in the Methods section were adapted from previous work by Stevenson et al. for angle-dependent CD measurements of gold nanocrescents in the visible spectral range.[21] Figure 1e presents the FTIR (top), VCD (middle), and VCD noise (bottom) spectra for an array of 2.00-μm-diameter NBHs at θ = 0° (black), θ = +30° (red), and θ = −30° (blue). Features common to all NBH arrays are observed. The FTIR spectrum for θ = 0° shows a single dominant LSPR peak response centered at 1951 cm^{-1} which red-shifted to 1857 cm^{-1} upon tilting at θ = ±30°, and an additional shoulder appeared centered at 2573 cm^{-1}. For the VCD analysis, no VCD response was observed for measurements at normal incidence (black spectrum centered at ΔA = 0), which is expected for a two-dimensional achiral structure. However, when the NBH substrate was tilted at θ = ±30°, CD responses, including a flip in the handedness with the tilt angle, were observed. At θ = +30° (red) and −30° (blue), two major VCD bands appeared centered at 2897 and 1990 cm^{-1}, referred to as VCD band 1 and VCD band 2, respectively. The handedness of the two VCD bands was opposite at a set angle, and both bands switched handedness when the substrate tilt angle was changed. For example, VCD band 1 had a positive, or left-handed, response for θ = +30° while VCD band 2 had a negative, or right-handed, response. At the other tilt angle (θ = −30°), VCD band 1 and VCD band 2 flipped to a right-handed response and a left-handed response, respectively. A VCD noise spectrum is presented in the bottom panel of Figure 1e. The lack of features demonstrates the optimization of the optical system and the absence of artifacts contributing to the VCD spectra for the NBHs. The observed VCD responses indicate that the NBHs exhibit extrinsic chiroptical behavior, as well as orientation-dependent handedness.[21,31,40] We expect the offset of the inner hole plays a major role in the CD behavior, similar to the concentric ring structures reported by Bochenkov et al.,[35] and the impact of the two- and three-dimensional structural features on the chiroptical response of the NBHs is being explored through finite-difference time-domain (FDTD) calculations.

The primary LSPR and CD band spectral positions were sensitive to the outer diameter of the NBH structures which was controlled by the size of the PS bead used in the NTL fabrication. The FTIR and VCD responses for NBHs with outer diameters of 1.75 ± 0.05, 2.00 ± 0.06, 2.30 ± 0.04, 2.79 ± 0.08 μm were measured. The full FTIR and VCD spectra are presented in Figure S2 in the Supporting Information. The center positions of the two primary VCD bands (labeled as VCD band 1 for the higher energy band and VCD band 2 for the lower energy band) and the primary LSPR band are plotted as a function of the outer NBH diameter in Figure 1f. The spectral positions of the LSPR band and both VCD bands shifted to lower energy as the outer diameter of the NBHs increased. This shift is expected due to the increase in size, and the approximately linear trend matches the size-dependent shifts for other fabricated plasmonic structures, such as rings, disks and crescents.[37,41−44] As observed in the plot in Figure 1f and in the spectra presented in Figure S2, the central position of both VCD band 1 and band 2 are offset from the peak of the primary LSPR band. Also, VCD band 1 exhibited a greater sensitivity to the change in diameter compared to the LSPR peak and VCD band 2. The dependence of these optical responses on structural properties of the NBHs is being explored with FDTD simulations.

https://doi.org/10.1021/acs.jpcc.4c04448
J. Phys. Chem. C 2024, 128, 15091−15102

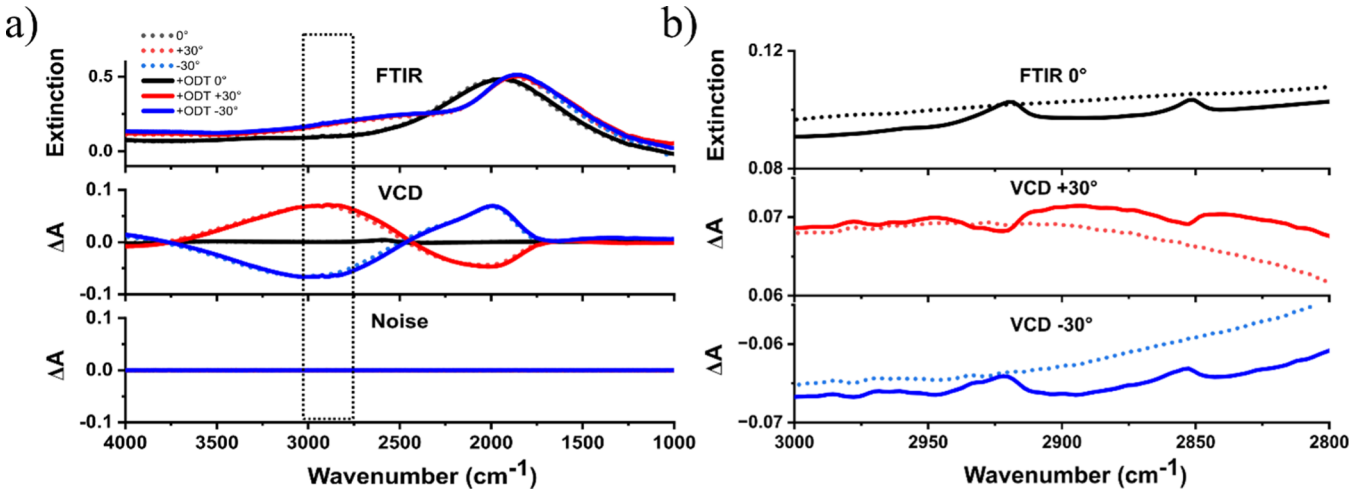

Figure 2. (a) FTIR, VCD, and noise spectra of an array of 2.00 μm NBHs before and after adsorption of ODT. (b) Expanded region of the FTIR and VCD spectra outlined by the dotted line rectangle in (a) focused on the methylene stretching region. All spectra were collected for NBHs without ODT (dotted lines) and with ODT adsorbed (solid lines) at incident angles of θ = 0° (black), θ = +30° (red), and θ = −30° (blue).

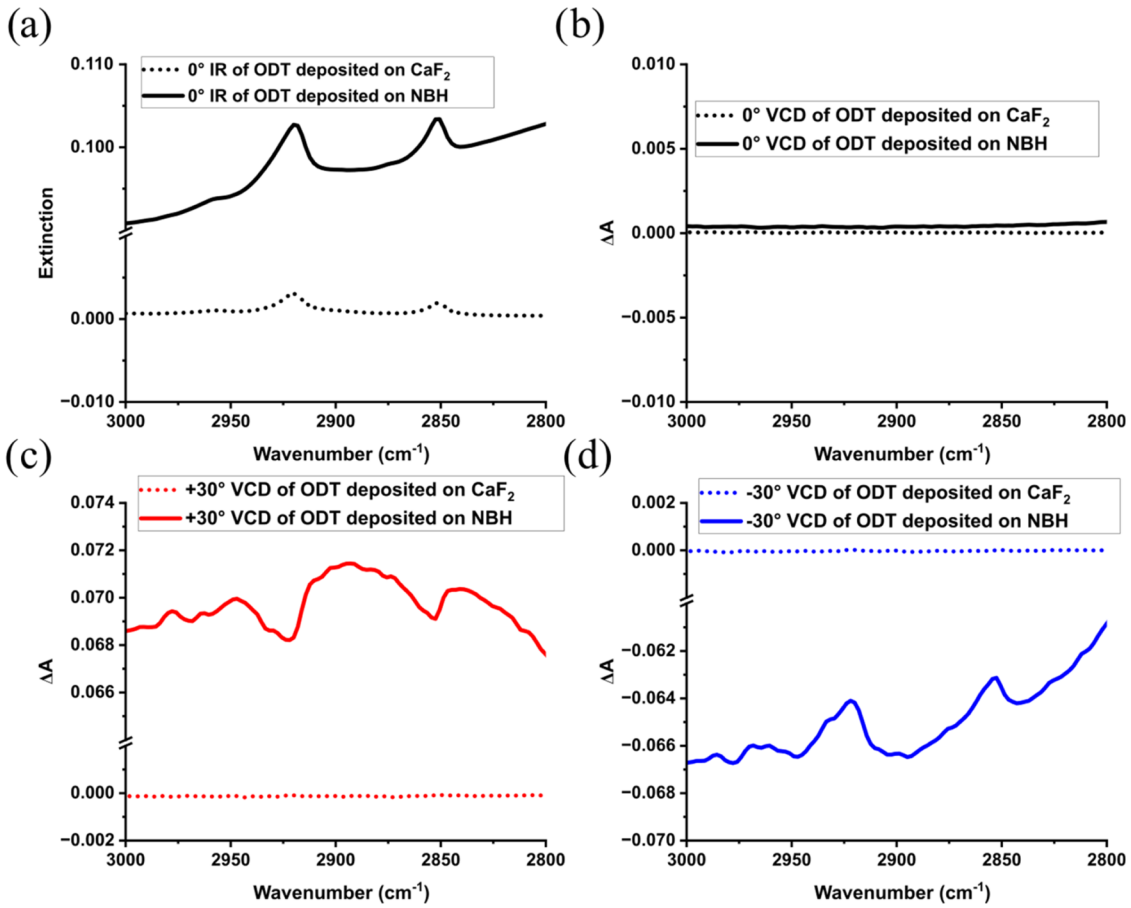

Figure 3. FTIR and VCD spectra of ODT on 2.00 μm Au NBHs and a CaF_2 substrate. (a) FTIR spectra collected at normal incidence (θ = 0°). VCD spectra collected at (b) normal incidence (θ = 0°) and at out-of-plane tilt angles of (c) θ = +30°, and (d) θ = −30°.

Control of the LSPR and chiroptical behavior of NBH structures was used to investigate the influence of the plasmonic structures on the VCD spectra of ODT molecules. Notably, the extrinsic chiroptical response provided an approach to manipulate (i.e., turn on and off chiroptical response and control handedness) the CD responses of the NBHs by simply controlling the tilt angle (θ) of the substrate with respect to the incident circularly polarized light. FTIR and VCD spectra were collected at normal (θ = 0°) and tilted (θ = ±30°) incident angles before and after adsorption of ODT on NBHs. Figure 2a presents FTIR, VCD, and VCD noise spectra for an array of 2.00 μm NBHs without ODT (dotted lines) and after adsorption of ODT (solid lines). A 15−25 cm^{-1} red-shift was observed for the LSPR bands and VCD bands after

https://doi.org/10.1021/acs.jpcc.4c04448
J. Phys. Chem. C 2024, 128, 15091−15102

adsorption of ODT relative to the bare NBHs. The red-shift of the plasmonic response with the adsorption of the ODT molecules is due to the change in the refractive index.[45−47] Except for the peak shifts, no significant spectral changes were observed. The shape and amplitude of the LSPR and VCD bands are largely unchanged by the addition of ODT. This observation is in contrast to reports where a chiral molecule significantly changed the shape and spectral position (by more than 25 cm^{-1}) of the CD responses of achiral or chiral plasmonic nanostructures.[27,48]

Although the addition of ODT had minimal impact on the optical responses of the plasmonic structures, the influence of the chiroptical behavior of the NBHs on the ODT VCD spectrum was significant. Figure 2b presents an expanded view of a smaller spectral region of the FTIR and VCD spectra for ODT on the NBHs from panel (a). The top panel presents the FTIR spectrum of ODT on 2.00 μm NBHs measured at normal incidence (θ = 0°). Vibrational bands for the methylene symmetric and antisymmetric stretch modes of ODT were observed at 2852 and 2920 cm^{-1}, respectively. The bands exhibited some asymmetry in the line shape, which is expected due to the proximity of the NBH LSPR band.[49] At normal incidence (θ = 0°), there was no VCD response, only featureless, flat lines, for the NBHs and the ODT molecules adsorbed on the NBHs (see spectra in Figure S3 in Supporting Information). However, for VCD spectra collected at tilt angles of θ = +30° (red) and θ = −30° (blue), VCD bands associated with the ODT methylene symmetric and antisymmetric stretch modes were observed, although the molecule is achiral. For the molecular VCD bands, the direction of the dip of the VCD band indicated the handedness. For a band dipping down, the change in ΔA was negative (−), indicating a right-handed response. For a band dipping up, the change in ΔA was positive (+), indicating a left-handed response. As observed, in Figure 2b, the handedness of the ODT VCD response flipped with the substrate tilt angle, which was used to manipulate the handedness of the CD response of the plasmonic structures. In addition, the handedness of the molecular VCD bands had an inverse relationship with the NBH CD response handedness. When the NBHs exhibited a left-handed (+) CD response, the ODT VCD band was right-handed (−). For the opposite situation, a right-handed (−) NBH VCD response, the molecular VCD response was left-handed (+). The change in handedness of the molecular VCD response with the change in handedness of the chiroptical response of the NBHs provides evidence the observed VCD response from the achiral molecules was influenced by the plasmonic structures. However, the potential for artifacts from the measurement approach contributing to the signals was considered.

The ODT VCD bands were only observed when the substrate with the NBHs was tilted. To determine if the observed molecular VCD bands were an artifact of tilting, ODT was deposited onto a bare CaF_2 substrate and angle-dependent FTIR and VCD measurements were made. Figure 3 shows the angle-dependent spectra of ODT on 2.00 μm NBHs and ODT drop cast on a bare substrate. The FTIR spectra at normal incidence (Figure 3a) show a decrease in the amplitude of the methylene vibrational bands for the ODT deposited on the bare CaF_2 substrate (dotted line) compared to ODT on the NBH array (solid line), even though the number of molecules is smaller on the NBHs, due to plasmonic surface-enhanced infrared absorption (SEIRA) effects.[49,50] Also, the line shapes for ODT on CaF_2 are symmetric compared to ODT on the plasmonic structures, where the asymmetry is due to the proximity of the LSPR band. For VCD spectra collected at normal incidence (Figure 3b), no bands were observed for ODT deposited on the NBHs or the CaF_2 substrate. As expected, based on the previous analysis, VCD bands were observed for ODT on NBH arrays for incident angles of θ = +30° (Figure 3c) and θ = −30° (Figure 3d). However, for VCD analysis of ODT on the CaF_2 substrate, no bands were observed for any of the measurements, including when the substrate was tilted. The lack of VCD response at tilted incident angles for ODT deposited on CaF_2 indicates that the VCD bands observed for ODT on NBH arrays were not an artifact of tilting the substrate, but rather due to the influence of the plasmonic structures.

As observed in the VCD spectra in Figures 2b and 3c,d, the line shape of the ODT VCD bands has character of a Fano resonance, often observed in SEIRA and other plasmon-based spectroscopy methods.[50−53] This asymmetry in molecular bands due to Fano resonance is described by[49]

$$I \propto \frac{(q\gamma + \omega - \omega_0)^2}{(\omega - \omega_0)^2 + \gamma^2} \quad (1)$$

where I is the signal amplitude, γ is the molecular resonance bandwidth, ω_0 and ω are the frequencies of the resonant mode and the incident irradiation, respectively, and q is the Fano asymmetry parameter. The original purpose of the Fano formalism in eq 1 was to model the asymmetric line shapes for the discrete resonances of the autoionization of atoms observed as a result of interference between the resonance of the transition to the discrete state and the resonance of the transition to the continuum.[54] The asymmetry parameter, q, was attributed to the ratio of the transition probabilities to the discrete state and to the continuum. At very high values of the asymmetry parameter, transition to the continuum is very weak and a transition to the discrete state is very probable creating a resonance that is more Lorentzian in character. When the asymmetry parameter is close to unity, there is equal probability of transition to the continuum and the discrete state, and an asymmetric profile is observed.

In SEIRA, the interference that produces the asymmetric Fano line shape is between the broad plasmonic response and a comparatively narrow molecular absorption. In the case of the asymmetric ODT VCD bands, the narrow component may be related to the phase of the IR-absorbing vibrational transition or an influence of the electromagnetic near field of the NBHs on the vibrational modes, or possibly a combination. The VCD measurement is sensitive to phase changes, but molecular VCD bands only appear when there is a CD response, like in the case of chiral molecules. For ODT, the VCD bands were observed only for ODT on the plasmonic NBHs at θ = ±30°, when the NBHs exhibited an extrinsic CD response. To explore the origin of the VCD bands and the line shapes, the influence of the chiroptical responses of the NBHs was studied by tuning the spectral ranges of those plasmonic responses. The angle-dependent VCD spectra of ODT on NBH structures with four different diameters, ranging from 1.75 to 2.79 μm were collected. Representative SEM images of the NBHs are presented in Figure S1 in the Supporting Information. Using this NBH diameter range, the spectral positions of VCD band 1, VCD band 2 and the LSPR peaks were tuned and detuned relative to the spectral region of the ODT methylene stretch vibrational bands. The LSPR and

https://doi.org/10.1021/acs.jpcc.4c04448
J. Phys. Chem. C 2024, 128, 15091−15102

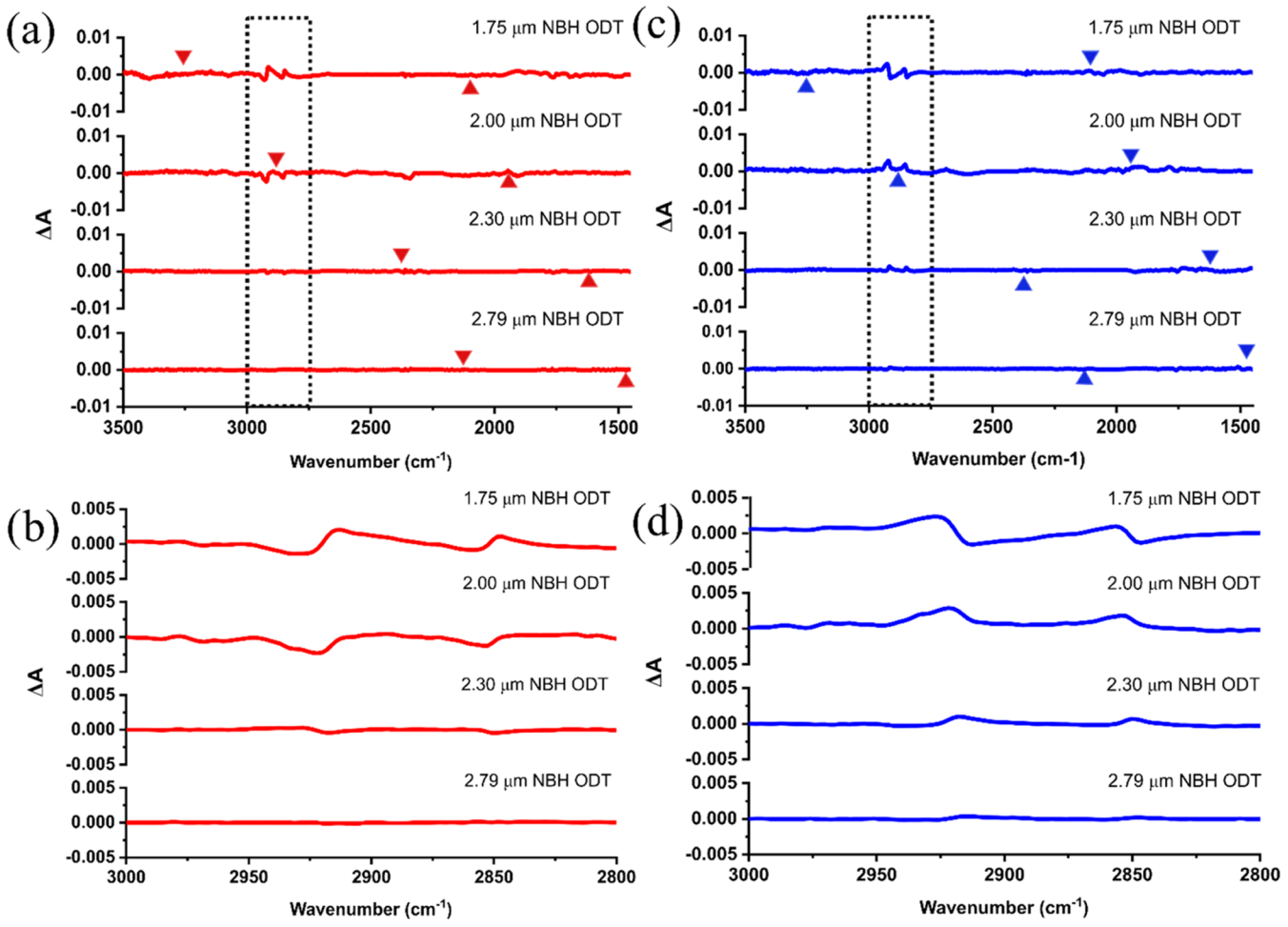

Figure 4. VCD spectra collected for ODT on NBHs at tilt angles of θ = +30° (a and b) and θ = −30° (c and d). A multipoint fit was used for background correction to remove the plasmonic CD responses. For a and b, the triangles indicate the center of the NBH CD bands, with the triangles above the spectrum indicating a left-handed CD response and the triangles below indicating a right-handed CD response. The spectral regions in the dotted line rectangles in (a) and (b) are presented in c and d to focus on the methylene stretching region for ODT.

VCD spectra measured at different tilt angles (θ = 0, +30, or −30°) before and after addition of ODT are presented in Figure S2 in the Supporting Information. As discussed previously (Figure 1f), the spectral positions of the LSPR and VCD bands shifted to lower energy as the NBH diameter increased. To focus on the influence of the CD response of the NBH structures on the molecular VCD bands, the background-corrected VCD spectra for ODT measured at substrate angles of θ = +30° and −30° are plotted in Figure 4a,b, respectively. To indicate the spectral positions of the NBH VCD bands and the handedness, triangles demarcate the center of the VCD bands with triangles above (apex pointing down) indicating a left-handed plasmonic CD response and triangles below (apex pointing up) indicating a right-handed plasmonic CD response. As shown in the spectra, the appearance of the ODT VCD bands depended on the relative position of the NBH VCD bands, most obviously VCD band 2. When the NBH VCD band 2 (i.e., the higher energy triangle position) was overlapping with the spectral region of the ODT methylene symmetric and antisymmetric stretch vibrational bands, the corresponding molecular VCD bands were observed in the spectra. However, when VCD band 2 was tuned to lower energy, for example in the case of the 2.79 μm NBH structures, ODT VCD bands were not observed. In fact, for the 2.79 μm NBHs, the entire VCD band 2 was shifted away from the methylene vibration spectral region (see Figure S2c in the Supporting Information), leading to the absence of bands in the VCD spectra in Figure 4a,b for those large structures. This effect of tuning and detuning CD band 2 was observed for both tilt angles (θ = +30 and −30°), as shown in Figure 4.

The shape of the ODT VCD bands also appeared to depend on the position of the NBH VCD band 2. To more clearly see the line shape changes of the ODT methylene bands, the regions outlined by the dotted line rectangle in Figure 4a,b were expanded in Figure 4c,d. For ODT deposited on the 1.75 μm NBHs and measured at θ = +30° (Figure 4a), the nearest NBH VCD band (i.e., VCD band 2) was centered at 3313 cm^{-1}, on the higher energy side of the methylene vibrational bands. Note, the NBH VCD response was still considerably overlapping with the molecular vibrational bands, despite the shift of the center of the band to a higher energy region (see full spectra in Figure S2 in the Supporting Information). Examining the line shape of the methylene bands in the spectrum in Figure 4c, the higher energy side of each molecular band was broadened compared to the lower energy side. The asymmetry in the line shape was mirrored for the methylene bands in the VCD spectrum collected at θ = −30° as shown in Figure 4d, where the sign is opposite ($-\Delta A$), but the shape is similar to broadening on the higher energy side. Similar asymmetry of the bands was observed for ODT on the 2.00

https://doi.org/10.1021/acs.jpcc.4c04448
J. Phys. Chem. C 2024, 128, 15091−15102

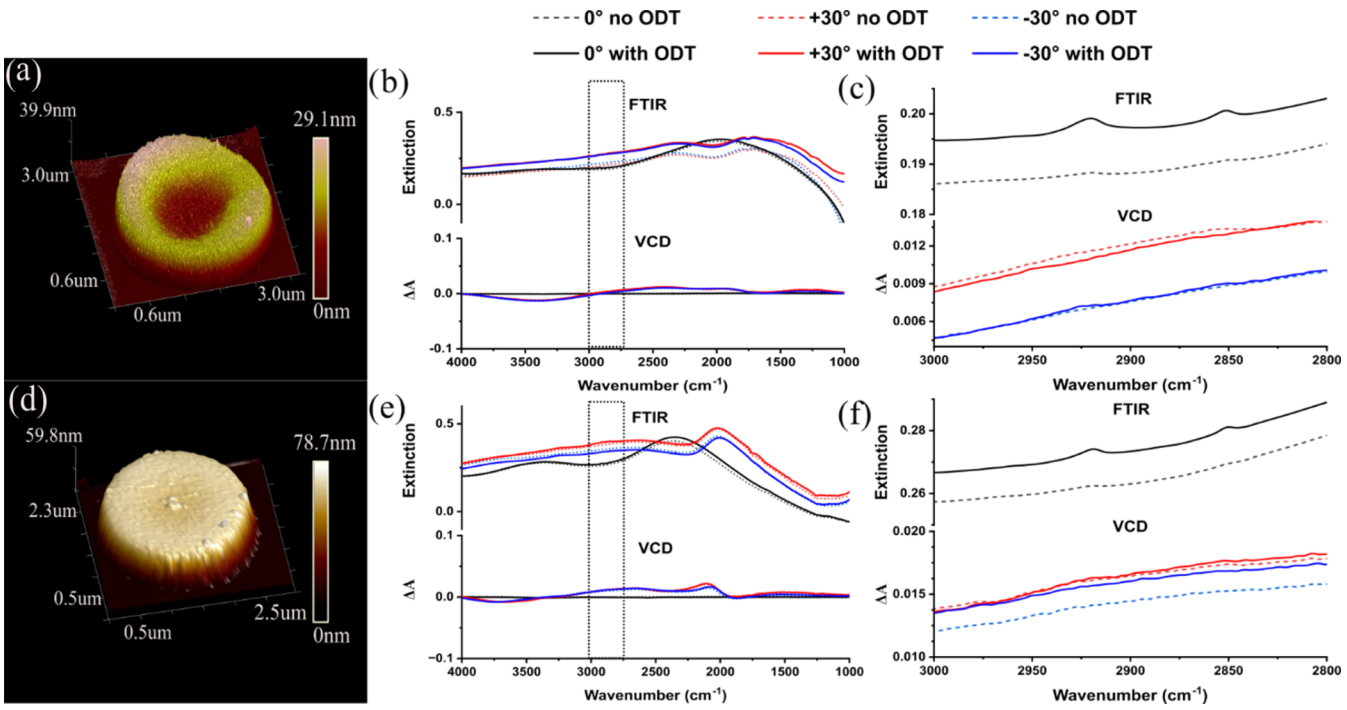

Figure 5. Structural and optical characterization of NB and ND structures. SEM images of (a) NBs and (d) NDs. Angle-dependent (θ = 0, +30, and −30°) FTIR and VCD spectra for NBs (b, c) and NDs (e, f) without ODT (hashed lines) and with ODT (solid lines). Spectral regions outlined by the hashed perimeter in (b) and (c) are plotted in (e) and (f) for the NBs and NDs, respectively.

and 2.30 μm NBHs, with decreasing amplitude as the NBH VCD band 2 shifted to lower energy where there was less overlap with the methylene vibrational bands. For the 2.79 μm NBHs, VCD band 2 was shifted out of the spectral range and VCD bands were not observed, as already mentioned.

The important role of the CD response of the NBHs in the observation of the molecular VCD bands is clear, but the different contributions of the LSPR and CD responses to the near field of the NBHs and the influence on the VCD spectra should be considered. In studying slit arrays, Knipper et al. also reported observations of VCD bands for achiral molecules (CO_2 and polyethylene).[27] In a brief discussion of electromagnetic field simulations in the Supporting Information, the authors attributed the origin of the VCD bands to SEIRA enhancement factors based on different near-field enhancements. Simulations of a polyethylene film on angled slit arrays showed a red-shift in the spectral position of the plasmonic mode accompanied by the appearance of vibrational bands that were attributed to the differential SEIRA enhancements for left- and right-circularly polarized light leading to a VCD spectrum. To explore the potential SEIRA effects in producing the ODT VCD spectra, the SEIRA spectra on the same NBHs were analyzed (see Figure S4 for spectra). For VCD, the strongest response (largest band amplitude) was observed for the NBHs with the most overlap with VCD band 2 for the 1.75 and 2.00 μm NBHs. In contrast, the strongest SEIRA response (i.e., enhancement factor of ∼12) was observed for ODT on the 2.30 μm NBHs. Also, the 1.75 and 2.79 μm NBHs had similar SEIRA enhancement factors of 5 and 6, respectively, but no VCD bands were observed for ODT on the 2.79 μm NBHs. The lack of correlation of the VCD spectra with the SEIRA enhancements for each size of NBH indicates there was not a strong dependence on the proximity to the dominant LSPR peak which impacted the SEIRA enhancement factors. Based on the studies of the different size NBHs, the NBH CD response played the more significant role in the ODT VCD spectra compared to SEIRA enhancements.

To further investigate the roles of the LSPR and chiroptical responses in producing the VCD spectra of ODT, two plasmonic structures with similar LSPR behavior, but without the substantial extrinsic chiroptical response of the NBHs were used as platforms for angle-based VCD spectroscopy measurements of ODT on the structures. Figure 5 presents AFM images of nanobowl (NB) and nanodisk (ND) plasmonic structures, and SEM images are presented in the Supporting Information (Figure S5). The AFM image of a NB in Figure 5a shows that the structure has a curved concave bowl shape matching the NBH structures, but without the hole exposing the CaF_2 substrate. Instead, the NB is a continuous gold structure fabricated by deposition of a thin gold film before addition of the PS bead template that forms the shape of the NB. Similarly, NDs were made by deposition of a thin gold film before adding the PS bead templates. The AFM image in Figure 5c shows that the ND is a circular structure with a flat surface.

The angle-dependent FTIR and VCD spectra of the NBs and NDs before and after addition of ODT are shown in Figure 5b,c,e,f. Although the NBs and NDs exhibit similar LSPR behavior as the NBHs, the VCD spectra in Figure 5b,e, show neither NBs nor NDs exhibit the strong extrinsic CD response of NBHs. At normal incidence (θ = 0°), no VCD response is observed from the structures. Although there are VCD responses at out-of-plane angles of θ = +30 and −30°, the amplitudes are much smaller (∼10×) compared to the VCD spectra for NBHs. Most notably, the NB and ND VCD spectra do not exhibit the distinct VCD bands sensitive to the tilt angle that would be indicative of extrinsic chiroptical behavior. Instead, the VCD spectra show small changes in

https://doi.org/10.1021/acs.jpcc.4c04448
J. Phys. Chem. C 2024, 128, 15091−15102

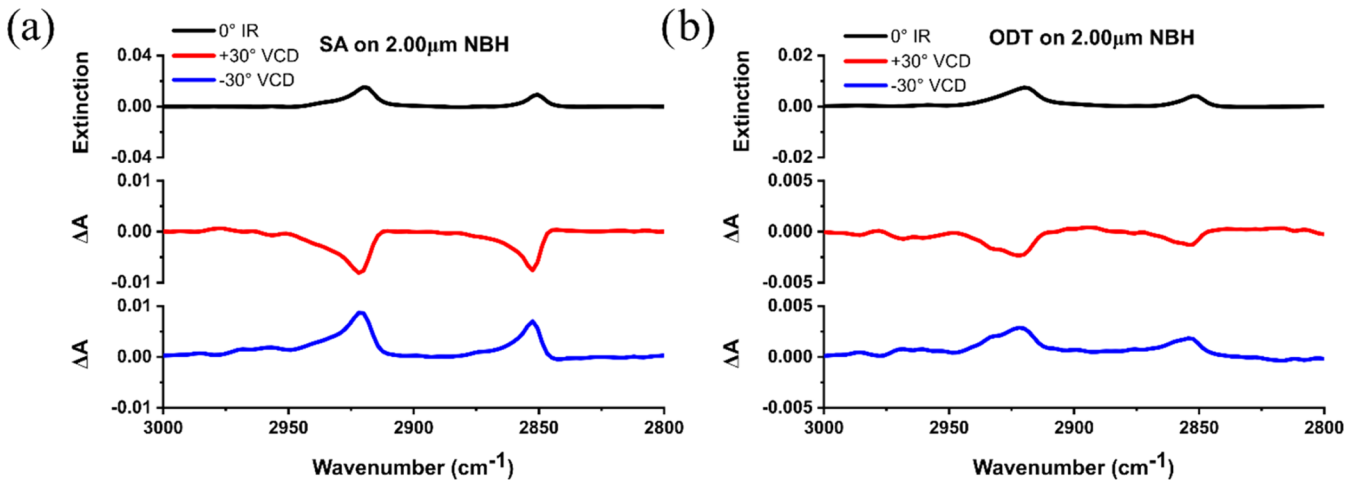

Figure 6. FTIR and VCD spectra for (a) SA drop cast and (b) ODT adsorbed on 2.00 μm NBHs. FTIR was collected for normal incidence (θ = 0°) (black) and VCD was collected at θ = +30° (red) and θ = −30° (blue). No bands were observed in the VCD spectra for normal incidence (data not shown). A multipoint fit was used for background correction to remove the plasmonic CD responses.

amplitude without a change in handedness for the different tilt angles (see Figure S5 for spectral details using a rescaled *y*-axis in the Supporting Information). Linear dichroism likely contributes to the small VCD signals observed at $\theta = \pm 30°$, in addition to small CD responses due to anisotropy in the structures, especially the contoured NBs. However, the strong extrinsic CD responses observed in the NBHs were not observed, further demonstrating an important role of the hole in the NBHs influencing the electric and magnetic fields and the electromagnetic coupling that produces CD activity in the NBH structures. It is suspected that linear dichroism also contributes to the background of the NBH VCD spectra, but those signals cannot be easily deconvoluted from the strong extrinsic CD response of the structures. A small red-shift was observed after adsorption of ODT, but the shapes of the LSPR and VCD spectra for the NBs and NDs were relatively unchanged. The regions outlined by the dotted rectangles in Figure 5b,e are plotted in Figure 5c,f to focus on the methylene vibrational bands. Although methylene symmetric and antisymmetric stretch bands were observed in the FTIR spectra for ODT on the NBs and NDs, distinct bands were not observed in the VCD spectra, contrary to what was observed for ODT on NBHs. The lack of VCD response for ODT on NBs and NDs provides more evidence of the role of the strong CD response of the NBHs in producing the VCD response from the ODT molecules.

To probe the role of the thiol-gold surface interaction or the organization of the ODT monolayer on the observed VCD bands and origin of the NBH influence on the achiral molecules, VCD measurements using the NBH platform were repeated with stearic acid (SA). SA is a structural analog of ODT with the same alkyl chain, but with a carboxylic acid instead of thiol terminal group. Rather than adsorbing in a specific manner through a thiol-gold interaction and forming an organized layer on the gold NBHs, SA was drop cast to form a disorganized, thin film. Figure 6a shows the normal incidence FTIR spectra, and the θ = +30° and the θ = −30° VCD spectra in red and blue, respectively. Considering the VCD spectra for both ODT and SA deposited on the NBH structures, the only difference between the responses is the higher amplitude observed for the methylene stretch vibrational bands in the SA spectrum in Figure 6a compared to the bands in the ODT spectrum in Figure 6b. A 1 mM solution of SA in ethanol was drop cast onto the surface of the NBH array and the ethanol was allowed to evaporate completely before measurement without any subsequent rinsing step. As a result, the concentration of SA on the surface of the NBHs was much higher than that of ODT (monolayer coverage). Overall, VCD spectra with similar line shapes were observed for molecules with different structural organization and interactions with the gold nanostructure surface. This further indicates that the origin of the VCD bands is not related to the organization of the molecules based on the very different situation for the SA and ODT molecules in this case or the molecule-gold surface interactions as others have postulated in other reports of chiral transfer.[55] The observations also provide further evidence in support of a mechanism based on a Fano-like interference due to the overlap of the vibrational bands for the molecule and the CD band of the plasmonic structures, which does not require the formation of a complex, the modification of surface chirality, or charge transfer. The observation of the VCD bands for SA in addition to ODT also emphasizes the important implications for developing an understanding of how plasmonic optical response may influence the VCD spectra of molecules in the development of plasmon-enhancement platforms for VCD spectroscopy.

Through the experimental studies, the unique role of the CD response of the NBHs in producing the ODT VCD bands was demonstrated by the tuning and detuning of the NBH CD bands and the lack of VCD response for ODT on the NBs and NDs, despite the similar LSPR behavior of those structures compared with NBHs. The observations indicate a major role of the chiroptical behavior of the NBHs. However, the mechanism is still not clear. The Fano line shape is similar to that observed in previous studies of chiral and achiral molecules coupling with plasmonic structures with chiroptical behavior. Govorov et al. posited that the mechanism of an observed chiral induction from an adsorbed chiral molecule to an achiral plasmonic mode was related to a Fano resonance, but suggested a different possible mechanism that depends on the polarization characteristics of the light and interactions with the plasmonic structures.[54−58] As discussed above, a Fano resonance is observed in both quantum mechanical and optical systems when a relatively finite or sharp absorption feature

https://doi.org/10.1021/acs.jpcc.4c04448
J. Phys. Chem. C 2024, 128, 15091−15102

interferes with a relatively continuous or broad absorption feature causing a characteristic asymmetry in the line shape of the sharp absorption feature which depends on the relative widths of the absorption features and their spectral position relative to one another.[54] As demonstrated, evidence of this type of interference effect is also observed in the VCD spectra from ODT on the NBHs based on the line shapes of the VCD bands and the dependence on the overlap with the CD responses of the NBHs.

One consideration for the origin of the discrete state that contributes to the Fano line shape may be the phase associated with the dipole oscillation for the vibrational transitions producing an interference with the plasmonic CD response. However, this would mean that the phase contributions did not cancel for right- vs left-circularly polarized light in the VCD measurements of ODT on NBHs with extrinsic chiroptical behavior. The observed VCD bands indicate a possible influence of the near-field electric and magnetic dipole moments of the plasmonic structures on the IR transition dipole moments of the ODT. A dependence on the near field conditions may help explain not only the observation of VCD bands, but also the dependence of the handedness of the molecular modes with respect to the CD handedness of the NBHs. Consider that the CD response of a molecular transition is proportional to the rotational strength[59]

$$\mathrm{CD}_{12} \propto \mathrm{Im}[\mu_{12} \cdot m_{12}] \tag{2}$$

where μ_{12} is the electric transition moment for a molecule from initial state 1 to final state 2, m_{12} is the magnetic transition dipole moment for the same transition, and Im denotes the imaginary component of the argument within the brackets. Upon examination of eq 2, for optical response in a system to be nonzero, the electric and magnetic transition dipole moments must be nonorthogonal according to the definition of a dot product. Accordingly, an electric or magnetic dipole in an electric or magnetic field will experience a torque with potential energy that is greatest when the dipole is perpendicular to the field and minimal when the dipole is aligned with the field[60]

$$\tau_E = \mu \times E \tag{3}$$

$$\tau_B = m \times B \tag{4}$$

where τ_E and τ_B are the torque experienced by an electric dipole (μ) in an electric field (E) or a magnetic dipole (m) in a magnetic field (B), respectively. Therefore, the appearance of a VCD band corresponding to the molecular methylene stretching mode of ODT in the near-field environment of a NBH structure when a chiral plasmonic mode is excited could be explained by the alignment of the electric and magnetic transition dipole moments for those modes with the chiral plasmonic near fields. Since the rotational strength from eq 2 is proportional to the CD amplitude, the overall electric and magnetic transition dipoles of the chiral plasmonic near fields must be overall nonorthogonal, and, therefore, alignment with these near fields would produce an overall nonorthogonality between the electric and magnetic transition dipole moments for the methylene stretching modes of ODT. If the electric and magnetic transition dipole moments of ODT molecules were influenced by alignment with electric and magnetic fields of the chiral plasmonic modes, then a change in the sign of handedness of the plasmonic near field could impact the sign of the angle between the electric and magnetic transition dipole moments of ODT would as well. This could account for the change in the handedness of the chiral response observed in ODT when the handedness of the NBH chiral plasmonic mode is switched. The influence of the near-field environment on the VCD response of the achiral ODT molecules through perturbing the IR transitions could be considered a form of chiral transfer. This possible mechanism for producing a polarization-dependent discrete state that contributed to the Fano resonance is similar to the chiral transfer from a chiral plasmonic mode to an achiral molecule demonstrated experimentally for circularly polarized fluorescence.[61] Banik et al. also reported chiral transfer related to the orientation-dependent handedness of a chiral plasmonic nanoparticle dimer that produced Raman optical activity (ROA) from achiral molecules in surface-enhanced Raman spectroscopy measurements.[40] The ROA from the molecules followed the chiroptical behavior of the plasmonic antennas that was tuned over a continuum of left-handed to right-handed plasmonic CD responses. This influence of the chiroptical activity of the plasmonic antenna was similar to the impact of tuning the CD band of the NBHs relative to the spectral range of the ODT vibrational bands, where the vibrational bands disappeared in the absence of plasmonic chiroptical activity.

CONCLUSIONS

In this work, extrinsically chiral gold NBH structures were introduced as a platform to investigate the influence of the CD responses of the NBHs on the VCD spectra of ODT. The amplitude, handedness, and line shape of symmetric and antisymmetric methylene stretch bands in the VCD spectra of ODT were found to depend on the spectral overlap and the handedness of the CD bands of the NBHs. The lack of molecular VCD bands for ODT on NBs and NDs with similar LSPR responses, but without the extrinsic chiroptical behavior of NBHs, demonstrated the influence of the plasmonic CD response compared to SEIRA enhancements. VCD bands observed for SA and ODT, two structural analogs with different functional groups, demonstrated the influence of the plasmonic nanostructures on molecules with different surface interactions and organization. The role of the NBH CD responses and the relationship of the molecular VCD bands to Fano resonance were explored. The asymmetric line shapes indicated an interference process that may be due to interactions of the plasmonic near field with the electric and magnetic transition dipole moments of the vibrational transitions of the achiral molecules. Future studies will probe the origin of the molecular VCD response from achiral molecules. Further investigation of the coupling between plasmonic nanostructures with varying degrees of structural anisotropy with a variety of achiral and chiral molecules will be key to determining the mechanisms involved. A better understanding of the influence of plasmonic platforms on molecular VCD spectra is essential for applications of plasmon-enhanced VCD analysis for chiral drug therapy design, chiral molecule synthesis assessment, and assignment of absolute configuration.

ASSOCIATED CONTENT

Supporting Information

The Supporting Information is available free of charge at https://pubs.acs.org/doi/10.1021/acs.jpcc.4c04448.

https://doi.org/10.1021/acs.jpcc.4c04448
J. Phys. Chem. C 2024, 128, 15091−15102

SEM image of NBHs with different diameters; FTIR and VCD spectra for NBHs with different diameters; VCD spectra collected at normal incidence for NBH with and without ODT; SEIRA spectra for ODT on NBHs with different diameters; discussion of SEIRA enhancement factors; SEM images and FTIR and VCD spectra for NBs and ND (PDF)

AUTHOR INFORMATION

Corresponding Author

Jennifer S. Shumaker-Parry − *Department of Chemistry, University of Utah, Salt Lake City, Utah 84112, United States;* orcid.org/0000-0003-0357-1792; Email: shumaker-parry@chem.utah.edu

Authors

Amy Morren − *Department of Chemistry, University of Utah, Salt Lake City, Utah 84112, United States*

Aria T. Ballance − *Department of Chemistry, University of Utah, Salt Lake City, Utah 84112, United States*

Flore K. Elliott − *Department of Chemistry, University of Utah, Salt Lake City, Utah 84112, United States*

Complete contact information is available at: https://pubs.acs.org/10.1021/acs.jpcc.4c04448

Notes

The authors declare no competing financial interest.

ACKNOWLEDGMENTS

This material is based upon work supported by the National Science Foundation under Grant No. CHE-2004183. A.M. was supported in part by the National Science Foundation Graduate Research Fellowship under Grant No. 2139322. Materials Research-Photonic Materials Division. A.T.B. was supported in part by a fellowship award under contract FA9550-21-F-0003 through the National Defense Science and Engineering Graduate (NDSEG) Fellowship Program, sponsored by the Air Force Research Laboratory (AFRL), the Office of Naval Research (ONR) and the Army Research Office (ARO). F.K.E. was supported in part by NSF REU 2150526. This work made use of Nanofab EMSAL shared facilities of the Micron Technology Foundation Inc. Microscopy Suite sponsored by the John and Marcia Price College of Engineering, Health Sciences Center, Office of the Vice President for Research. This work was performed in part at the Utah Nanofab Cleanroom sponsored by the John and Marcia Price College of Engineering College of Engineering and the Office of the Vice President for Research. The authors appreciate the support of the staff and facilities that made this work possible. We gratefully acknowledge Jordan Nafie at Biotools, Inc. for discussions and assistance with the instrument configuration.

REFERENCES

(1) Blackmond, D. G. The origin of biological homochirality. *Cold Spring Harbor Perspect. Biol.* **2010**, *2*, No. a002147.

(2) Vantomme, G.; Crassous, J. Pasteur and chirality: A story of how serendipity favors the prepared minds. *Chirality* **2021**, *33*, 597−601.

(3) Smith, S. W. Chiral toxicology: It's the same thing···Only different. *Toxicol. Sci.* **2009**, *110*, 4−30.

(4) Inoue, Y.; Ramamurthy, V. *Chiral Photochemistry*; CRC Press, 2004; p 3.

(5) Ward, T. J.; Ward, K. D. Chiral separations: A review of current topics and trends. *Anal. Chem.* **2012**, *84*, 626−635.

(6) Berova, N.; Di Bari, L.; Pescitelli, G. Application of electronic circular dichroism in configurational and conformational analysis of organic compounds. *Chem. Soc. Rev.* **2007**, *36*, 914−931.

(7) Keiderling, T. A. Structure of condensed phase peptides: Insights from vibrational circular dichroism and raman optical activity techniques. *Chem. Rev.* **2020**, *120*, 3381−3419.

(8) Magyarfalvi, G.; Tarczay, G.; Vass, E. Vibrational circular dichroism. *Wiley Interdiscip. Rev.: Comput. Mol. Sci.* **2011**, *1*, 403−425.

(9) Freedman, T. B.; Cao, X.; Dukor, R. K.; Nafie, L. A. Absolute configuration determination of chiral molecules in the solution state using vibrational circular dichroism. *Chirality* **2003**, *15*, 743−758.

(10) Setnička, V.; Urbanová, M.; Bouř, P.; Král, V.; Volka, K. Vibrational circular dichroism of 1,1′-binaphthyl derivatives: Experimental and theoretical study. *J. Phys. Chem. A* **2001**, *105*, 8931−8938.

(11) Kurouski, D. Advances of vibrational circular dichroism (VCD) in bioanalytical chemistry. A review. *Anal. Chim. Acta* **2017**, *990*, No. 54e66.

(12) Nafie, L. A. *Vibrational Optical Activity: Principles and Applications*; John Wiley & Sons, 2011; pp 169−204.

(13) Nafie, L. A.; D, R. K. Vibrational optical activity in chiral analysis. In *Chiral Analysis: Advances in Spectroscopy, Chromatography and Emerging Methods*; Polavarapu, P. L., Ed.; Elsevier Science, 2018; pp 201−247.

(14) Frank, B.; Yin, X.; Schäferling, M.; Zhao, J.; Hein, S. M.; Braun, P. V.; Giessen, H. Large-area 3D chiral plasmonic structures. *ACS Nano* **2013**, *7*, 6321−6329.

(15) Wang, Y.; Xu, J.; Wang, Y.; Chen, H. Emerging chirality in nanoscience. *Chem. Soc. Rev.* **2013**, *42*, 2930−2962.

(16) Xu, H. X.; Wang, G. M.; Qi, M. Q.; Cai, T.; Cui, T. J. Compact dual-band circular polarizer using twisted hilbert-shaped chiral metamaterial. *Opt Express* **2013**, *21*, 24912−24921.

(17) Tullius, R.; Karimullah, A. S.; Rodier, M.; Fitzpatrick, B.; Gadegaard, N.; Barron, L. D.; Rotello, V. M.; Cooke, G.; Lapthorn, A.; Kadodwala, M. "Superchiral" spectroscopy: Detection of protein higher order hierarchical structure with chiral plasmonic nanostructures. *J. Am. Chem. Soc.* **2015**, *137*, 8380−8383.

(18) Zhao, Y.; Askarpour, A. N.; Sun, L.; Shi, J.; Li, X.; Alu, A. Chirality detection of enantiomers using twisted optical metamaterials. *Nat. Commun.* **2017**, *8*, No. 14180.

(19) Wang, X.; Tang, Z. Circular dichroism studies on plasmonic nanostructures. *Small* **2017**, *13*, No. 1601115.

(20) Solomon, M. L.; Hu, J.; Lawrence, M.; García-Etxarri, A.; Dionne, J. A. Enantiospecific optical enhancement of chiral sensing and separation with dielectric metasurfaces. *ACS Photonics* **2019**, *6*, 43−49.

(21) Stevenson, P. R.; Du, M.; Cherqui, C.; Bourgeois, M. R.; Rodriguez, K.; Neff, J. R.; Abreu, E.; Meiler, I. M.; Tamma, V. A.; Apkarian, V. A.; Schatz, G. C.; Yuen-Zhou, J.; Shumaker-Parry, J. S. Active plasmonics and active chiral plasmonics through orientation-dependent multipolar interactions. *ACS Nano* **2020**, *14*, 11518−11532, DOI: 10.1021/acsnano.0c03971.

(22) Du, W.; Wen, X.; Gérard, D.; Qiu, C.-W.; Xiong, Q. Chiral plasmonics and enhanced chiral light-matter interactions. *Science China Physics, Mechanics & Astronomy* **2019**, *63* (4), No. 244201, DOI: 10.1007/s11433-019-1436-4.

(23) Warning, L. A.; Miandashti, A. R.; McCarthy, L. A.; Zhang, Q.; Landes, C. F.; Link, S. Nanophotonic approaches for chirality sensing. *ACS Nano* **2021**, *15*, 15538−15566.

(24) Fedotov, V. A.; Mladyonov, P. L.; Prosvirnin, S. L.; Rogacheva, A. V.; Chen, Y.; Zheludev, N. I. Asymmetric propagation of electromagnetic waves through a planar chiral structure. *Phys. Rev. Lett.* **2006**, *97*, No. 167401.

(25) Schäferling, M.; Dregely, D.; Hentschel, M.; Giessen, H. Tailoring enhanced optical chirality: Design principles for chiral plasmonic nanostructures. *Phys. Rev. X* **2012**, *2*, No. 031010.

(26) Smith, K. W.; Link, S.; Chang, W.-S. Optical characterization of chiral plasmonic nanostructures. *J. Photochem. Photobiol., C* **2017**, *32*, 40−57.
(27) Knipper, R.; Kopecký, V.; Huebner, U.; Popp, J.; Mayerhöfer, T. G. Slit-enhanced chiral- and broadband infrared ultra-sensing. *ACS Photonics* **2018**, *5*, 3238−3245.
(28) Xu, C.; Ren, Z.; Zhou, H.; Zhou, J.; Ho, C. P.; Wang, N.; Lee, C. Expanding chiral metamaterials for retrieving fingerprints via vibrational circular dichroism. *Light Sci. Appl.* **2023**, *12*, No. 154.
(29) Xu, C.; Ren, Z.; Zhou, H.; Zhou, J.; Li, D.; Lee, C. Near-field coupling induced less chiral responses in chiral metamaterials for surface-enhanced vibrational circular dichroism. *Adv. Funct. Mater.* **2023**, *34*, No. 2314482.
(30) Biswas, A.; Cencillo-Abad, P.; Shabbir, M. W.; Karmakar, M.; Chanda, D. Tunable plasmonic superchiral light for ultrasensitive detection of chiral molecules. *Sci. Adv.* **2024**, *10*, No. eadk2560.
(31) Plum, E.; Fedotov, V. A.; Zheludev, N. I. Extrinsic electromagnetic chirality in metamaterials. *J. Opt. A: Pure Appl. Opt.* **2009**, *11*, No. 074009.
(32) Efrati, E.; Irvine, W. T. M. Orientation-dependent handedness and chiral design. *Phys. Rev. X* **2014**, *4*, No. 011003.
(33) Cao, T.; Wei, C.-w.; Li, Y. Dual-band strong extrinsic 2D chirality in a highly symmetric metal-dielectric-metal achiral metasurface. *Opt. Mater. Express* **2016**, *6*, 303−311.
(34) Plum, E. Extrinsic chirality: Tunable optically active reflectors and perfect absorbers. *Appl. Phys. Lett.* **2016**, *108*, No. 241905.
(35) Bochenkov, V. E.; Klös, G.; Sutherland, D. S. Extrinsic chirality of non-concentric plasmonic nanorings. *Opt. Mater. Express* **2017**, *7*, 3715−3721.
(36) Wang, Y.; Qi, J.; Pan, C.; Wu, Q.; Yao, J.; Chen, Z.; Chen, J.; Li, Y.; Yu, X.; Sun, Q.; Xu, J. Giant circular dichroism of large-area extrinsic chiral metal nanocrecents. *Sci. Rep.* **2018**, *8*, No. 3351.
(37) Aizpurua, J.; Hanarp, P.; Sutherland, D. S.; Käll, M.; Bryant, G. W.; García de Abajo, F. J. Optical properties of gold nanorings. *Phys. Rev. Lett.* **2003**, *90*, No. 057401.
(38) Shumaker-Parry, J. S.; Rochholz, H.; Kreiter, M. Fabrication of crescent-shaped optical antennas. *Adv. Mater.* **2005**, *17*, 2131−2134.
(39) Nafie, L. A. Dual polarization modulation: A real-time, spectral-multiplex separation of circular dichroism from linear birefringence spectral intensities. *Appl. Spectrosc.* **2000**, *54*, 1634−1645.
(40) Banik, M.; R, K.; Hulkko, E.; Apkarian, V. A. Orientation-dependent handedness of chiral plasmons on nanosphere dimers: How to turn a right hand into a left hand. *ACS Photonics* **2016**, *3*, 2482−2489.
(41) Hanarp, P.; Käll, M.; Sutherland, D. S. Optical properties of short range ordered arrays of nanometer gold disks prepared by colloidal lithography. *J. Phys. Chem. B* **2003**, *107*, 5768−5772.
(42) Zorić, I.; Zäch, M.; Kasemo, B.; Langhammer, C. Gold, platinum, and aluminum nanodisk plasmons: Material independence, subradiance, and damping mechanisms. *ACS Nano* **2011**, *5*, 2535−2546.
(43) Bukasov, R.; Shumaker-Parry, J. S. Highly-tunable infrared extinction properties of gold nanoparticles. *Nano Lett.* **2007**, *7*, 1113−1118.
(44) Cooper, C. T.; Rodriguez, M.; Blair, S.; Shumaker-Parry, J. S. Mid-infrared localized plasmons through structural control of gold and silver nanocrescents. *J. Phys. Chem. C* **2015**, *119*, 11826−11832.
(45) Haes, A. J.; Van Duyne, R. P. A nanoscale optical blosensor: Sensitivity and selectivity of an approach based on the localized surface plasmon resonance spectroscopy of triangular silver nanoparticles. *J. Am. Chem. Soc.* **2002**, *124*, 10596−10604.
(46) Willets, K. A.; Van Duyne, R. P. Localized surface plasmon resonance spectroscopy and sensing. *Annu. Rev. Phys. Chem.* **2007**, *58*, 267−297.
(47) Balaur, E.; Sadatnajafi, C.; Abbey, B. Optical barcoding using polarisation sensitive plasmonic biosensors for the detection of self-assembled monolayers. *Sci. Rep.* **2022**, *12*, No. 13081.
(48) Maoz, B. M.; Moshe, A. B.; Vestler, D.; Bar-Elli, O.; Markovich, G. Chiroptical effects in planar achiral plasmonic oriented nanohole arrays. *Nano Lett.* **2012**, *12*, 2357−2361.
(49) Neubrech, F.; Huck, C.; Weber, K.; Pucci, A.; Giessen, H. Surface-enhanced infrared spectroscopy using resonant nanoantennas. *Chem. Rev.* **2017**, *117*, 5110−5145.
(50) Krauth, O.; Fahsold, G.; Magg, N.; Pucci, A. Anomalous infrared transmission of adsorbates on ultrathin metal films: Fano effect near the percolation threshold. *J. Chem. Phys.* **2000**, *113*, 6330−6333.
(51) Christ, A.; Ekinci, Y.; Solak, H. H.; Gippius, N. A.; Tikhodeev, S. G.; Martin, O. J. F. Controlling the Fano interference in a plasmonic lattice. *Phys. Rev. B* **2007**, *76*, 201405−201401−201404.
(52) Le, F.; Brandl, D. W.; Urzhumov, Y. A.; Wang, H.; Kundu, J.; Halas, N. J.; Aizpurua, J.; Nordlander, P. Metallic nanoparticle arrays: A common substrate for both surface-enhanced raman scattering and surface-enhanced infrared absorption. *ACS Nano* **2008**, *2*, 707−718.
(53) Hao, F.; Nordlander, P.; Sonnefraud, Y.; Van Dorpe, P.; Maier, S. A. Tunability of subradiant dipolar and Fano-type plasmon resonances in metallic ring/disk cavities: Implications for nanoscale optical sensing. *ACS Nano* **2009**, *3*, 643−652.
(54) Fano, U. Effects of configuration interaction on intensities and phase shifts. *Phys. Rev.* **1961**, *124*, 1866−1878.
(55) Govorov, A. O.; Gun'ko, Y. K.; Slocik, J. M.; Gérard, V. A.; Fan, Z.; Naik, R. R. Chiral nanoparticle assemblies: Circular dichroism, plasmonic interactions, and exciton effects. *J. Mater. Chem.* **2011**, *21*, 16806−16818.
(56) Govorov, A. O.; Fan, Z.; Hernandez, P.; Slocik, J. M.; Naik, R. R. Theory of circular dichroism of nanomaterials comprising chiral molecules and nanocrystals: Plasmon enhancement, dipole interactions, and dielectric effects. *Nano Lett.* **2010**, *10*, 1374−1382.
(57) Govorov, A. O. Plasmon-induced circular dichroism of a chiral molecule in the vicinity of metal nanocrystals. Application to various geometries. *J. Phys. Chem. C* **2011**, *115*, 7914−7923.
(58) Neubrech, F.; Pucci, A.; Cornelius, T. W.; Karim, S.; García-Etxarri, A.; Aizpurua, J. Resonant plasmonic and vibrational coupling in a tailored nanoantenna for infrared detection. *Phys. Rev. Lett.* **2008**, *101*, No. 157403.
(59) Snatzke, G. Circular dichroism: An introduction. In *Circular Dichroism: Principles and Applications*, 2nd ed.; Woody, R. W., Ed.; John Wiley & Sons, Inc., 2000; p 34.
(60) Feynman, R. *The Feynman Lectures on Physics*; Addison-Wesley, 1965; pp 1−15.
(61) Le, K. Q.; Hashiyada, S.; Kondo, M.; Okamoto, H. Circularly polarized photoluminescence from achiral dye molecules induced by plasmonic two-dimensional chiral nanostructures. *J. Phys. Chem. C* **2018**, *122*, 24924−24932.

https://doi.org/10.1021/acs.jpcc.4c04448
J. Phys. Chem. C 2024, 128, 15091−15102